UCRL-ID-132605

Determination of the Open and Closed Porosity in an Immobilized Pu Ceramic Wasteform

Henry F. Shaw

September 29, 1998

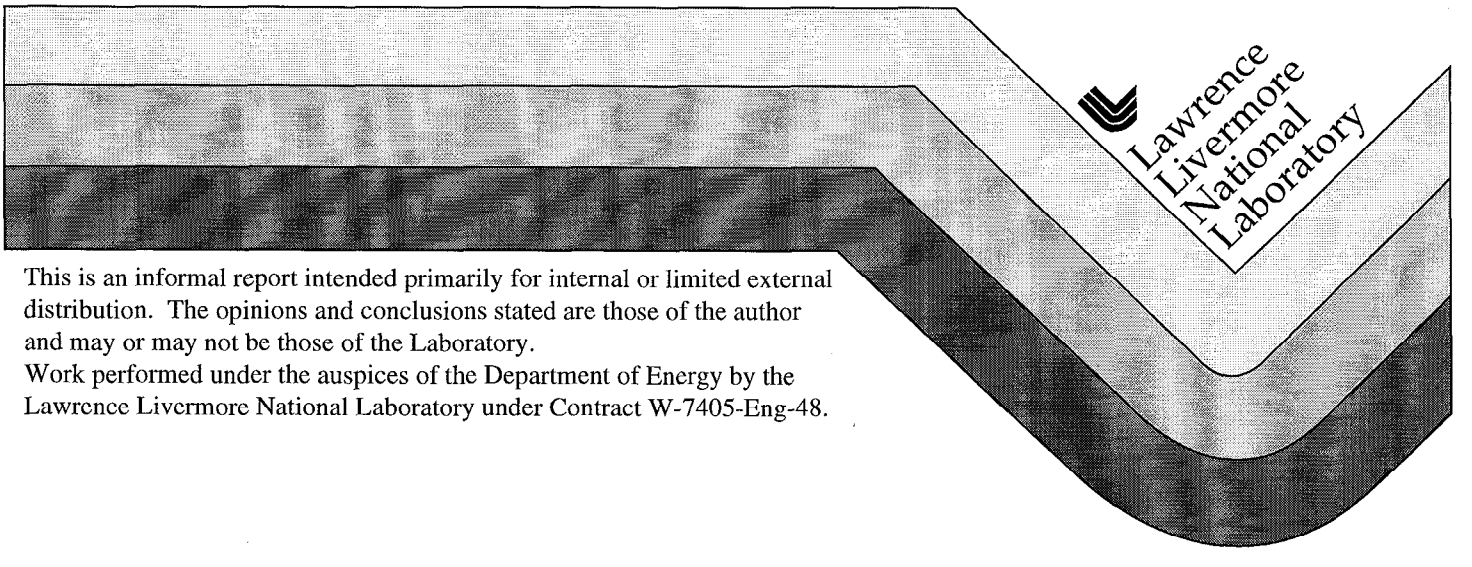

Work performed under the auspices of the Department of Energy by the Lawrence Livermore National Laboratory under Contract W-7405-Eng-48.

Determination of the Open and Closed Porosity in an Immobilized Pu Ceramic Wasteform

Henry F. Shaw

Plutonium Immobilization Project
September 29, 1998
Rev.0

Introduction

This purpose of this scoping study is to determine the relationship between the relative proportions of closed and open porosity as a function of total porosity in an analog ceramic under consideration for use in the disposition of surplus Pu. The sintered ceramic is expected to contain some residual porosity. Some fraction of this porosity will consist of isolated pores, and is referred to as the "closed porosity". The remainder of the pores will form an interconnected network that intersects the surface of the ceramic. This interconnected pathway will increase the surface area of the wasteform that is accessible to groundwater in a repository, though transport through this network is expected to be dominated by diffusive transport, with little or no advective transport.

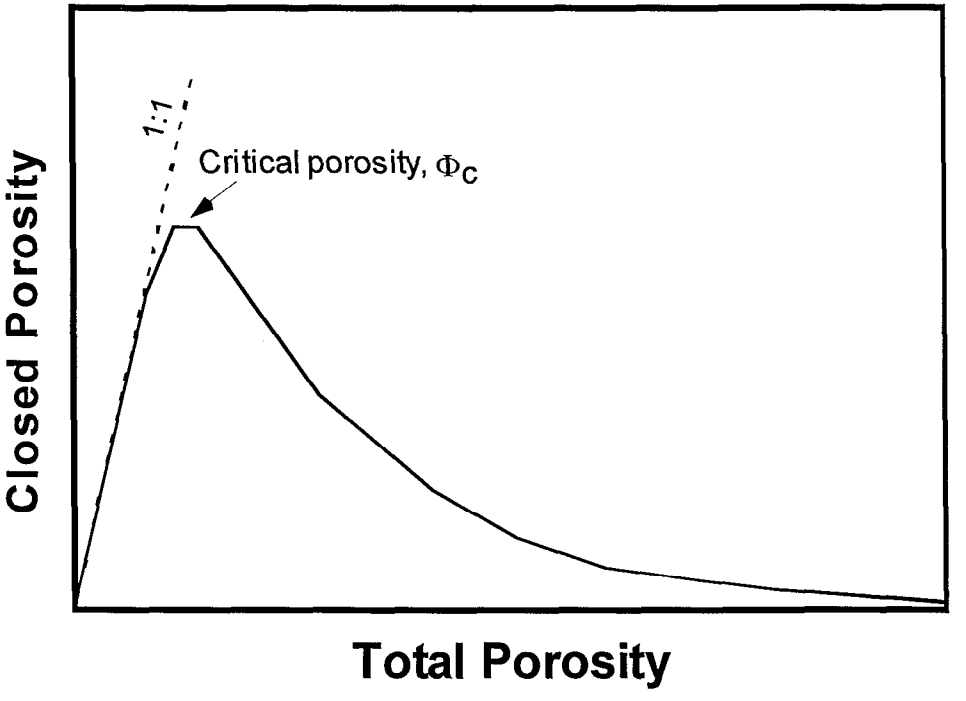

Figure 1. Schematic showing expected relationship between closed porosity and total porosity in a porous medium (*e.g.*, the Pu ceramic). Below the critical porosity, the closed porosity and total porosity are approximately equal.

In a porous medium, the fraction of porosity that is closed depends on the microstructure of the porosity (*e.g.*, the distribution of pore sizes, their geometry, their spatial distribution, their topology, *etc.*), as well as the total porosity of the sample. For a given microstructure, there will be a critical or "threshold" value of the total porosity at which an infinite interconnected network can form (see Isichenko, 1992). For typical ceramics and rocks this critical value lies between about 4 and 10% total porosity and is independent of the size of the system, so long as the system is much larger than the characteristic pore size. Below this critical value, essentially all the porosity is closed (except for the fraction of pores that lie at the surface of the material). Above the critical

value, the fraction of interconnected pores increases and must equal the total porosity at 100% porosity. Figure 1 schematically illustrates these relationships.

Samples and Procedures

Samples

A series of small Ce-analog ceramic samples having variable porosity were prepared by spacing the "green" ceramic pellets across the width of the sintering furnace. In this way, the pellets spanned the natural temperature gradient of the furnace; pellets at the center of the furnace were exposed to the highest (nominal) sintering temperature, while pellets at the sides of the cavity were exposed to lower temperatures. Two firings were made; one at a nominal temperature of 1350°C (series 178) and a second at a nominal temperature of 1400°C (series 183). Each firing held the pellets at temperature for 4 hours. The actual firing temperature of each pellet is unknown because the thermal gradient of the furnace chamber was not determined prior to the experiment. Suggestions for improvements in technique for future work are given at the end of this report.

The composition of the starting materials for these ceramics is given in Table 1. This material contains Ce^{4+} as a proxy or analog for both the U and Pu that will be present in the actual ceramic. This non-radioactive analog material is expected to have essentially the same pore structure and geometry of the actual Pu- and U-bearing final ceramic, and is thus acceptable for use in these measurements. If fully reacted, this material is expected to have a theoretical density (0% porosity) of approximately 5.4 g/cm^3. It is likely, however, that the samples sintered at lower temperatures are not fully reacted, and the theoretical density of the actual phase assemblage present should be somewhat lower than for the fully reacted material. A constant value of 5.4 g/cm^3 was assumed for all these samples, and this may introduce a small error in the porosity determinations of the high porosity samples. This effect is not of concern in the present study because we are primarily interested in the behavior of the porosity at relatively low values of total porosity (<10%), and these samples should approach a fully reacted state.

Table 1. Starting bulk composition of the Hf-Ce-Ce ceramic

Component	Mass (g)	Source
$Ca(OH)_2$	15.09	Alfa/AESAR
TiO_2 (anatase)	41.20	Aldrich
HfO_2	12.23	Teledyne Wah Chang grade S
Gd_2O_3	9.13	Pacific Industrial Development Corp. 99.99% min.
CeO_2	26.01	Molycorp

The volumes of the pellets were determined by measuring their overall dimensions. Because the pellets were not perfect cylinders, four measurements (spaced at 90° to one another) were made of the height of each pellet, and four similarly spaced measurements of the diameter were made. The height and diameter measurements were averaged and

used to calculate the geometric volume of the pellet. Calculating the standard deviation of the height and diameter measurements and propagating these errors through the volume calculation provided an estimate of the error on the volume measurement.

One additional sample ceramic composed of an older Zr-based formulation was used in this study. In this ceramic, Zr replaces Hf in the above formulation on a mole-for-mole basis. The sample used was an approximate rectangular prism cut from a ~2.625" diameter pellet. This material was used because it appeared to have a very low total porosity. As with the smaller pellets, the volume of the prism was calculated from measurements of the average height, width, and depth of the sample, with repeated measurements of each dimension providing an estimate of the error. If fully reacted, this material is expected to have a theoretical density (0% porosity) of approximately 4.92 g/cm^3.

Bulk density measurements

All samples were weighed to 0.0001 g. on an electronic balance that was calibrated using the balance's internal calibration routine prior to use. Bulk densities for the samples were then calculated using the geometric volume and mass. The results of all volume and bulk density measurements are given in Table 3.

Pycnometry measurements

For each sample, the volume occupied by solid material plus the volume of the closed porosity was determined using a helium pycnometer (Quantachrome Multipycnometer® model MVP-3). This device measures the volume of gas displaced by a sample by expanding a known reference volume of He gas at a known initial pressure into a sample chamber of known volume that contains the unknown sample. Assuming an ideal gas equation of state, the change in pressure upon expansion of the gas into the sample chamber can be related to the volume displaced by the sample:

$$V_s = V_c - V_r \cdot ((P_1/P_2)-1),$$

where

V_s is the volume displaced by the sample,
V_c is the (known) volume of the sample cell,
V_r is the (known) volume of the reference cell,
P_1 is the pressure measured before expansion into the sample cell,
P_2 is the pressure measured after expansion into the sample cell.

The Multipycnometer® was calibrated prior to use by following the manufacturer's instructions. Calibration entails the use of known volume spheres to determine the volumes of the reference and sample cells. The cell volumes determined by this

procedure were within 0.2% of the values reported by the manufacturer when the instrument was first received. This is considered excellent agreement.

Samples were run according to the manufacturer's recommended procedure in the smallest volume sample cell (the "micro" cell). The manufacturer recommends that this cell be used for the measurement of sample volumes between 0.5 and 4.5 cm^3. Most of the samples studied here had volumes somewhat less than 0.5 cm^3, and the measurement errors are consequently somewhat larger than could be obtained if larger samples were used.

Three sequential determinations of the volume were made for each sample, with the pressure reading of the expanded gas taken at approximately 15 seconds after opening the valve between the reference cell and sample cell. The results were averaged, and the standard deviation of the measurements calculated. The results are reported in Table 3 as the "Pycnometer volume". Densities were calculated using these volumes and the measured masses, and are reported in Table 3 as the "Pycnometer density"

To check whether 15 seconds was sufficient time to allow the gas pressure to equilibrate with the interior of the samples, several series of pressure measurements were made as a function of time. The first series of runs was made using sample P178-#10 (~26.7% total porosity) to see if the "final" pressure changed as a function of time. For the second series of measurements, the sample cell held a solid steel calibration sphere of approximately the same volume as the ceramic samples. These measurements provide a baseline for assessing the stability of the instrument over time. Some drift in the pressure reading is expected due to a combination of system leaks, which would result in a slow decrease in pressure, and fluctuations in the ambient temperature, which could result in either pressure increases or decreases, depending on whether the temperature was increasing or decreasing. The latter effect is expected to dominate, as a 1°C change in temperature at typical conditions (~23°C) would result in a 0.3% change in the measured pressure, which is well within the measurement sensitivity of the instrument. (In fact, a change of 0.05°C would result in a detectable pressure change.) The results of these measurements are presented in Table 2.

Table 2. Results of stability measurements of the Multipycnometer®

	Initial Pressure (psig)	"Final" pressure at X seconds								
		15s	30s	60s	90s	120s	180s	300s	420s	600s
Standard	17.298	7.100	7.101	7.103	7.105	7.108	7.111	7.117	7.120	7.126
"	17.172	7.039	7.038	7.036	7.035	7.034	7.033	7.033	7.032	7.032
"	17.233	7.069	7.068	7.068	7.067	7.067	7.066	7.066	7.065	7.065
P178-#10	17.533	6.909	6.909	6.909	6.910	6.910	6.911	6.913	6.914	6.917
"	18.111	7.141	7.141	7.142	7.142	7.143	7.144	7.144	7.145	7.147
"	no data	6.847	6.846	6.845	-	6.844	6.842	-	-	-

Figure 2 presents the same data, but expressed as the percentage change in the pressure relative to the pressure at 15 seconds. As can be seen, the pressure in the runs using the standard sphere both increased and decreased over the course of 10 minutes, though the maximum change was less than 0.4%. Changes of that magnitude can easily be explained by a small change in room temperature, which was not well controlled. The runs using the ceramic sample showed only small pressure changes, which were bracketed by the range of changes observed in the standard runs. Furthermore, there was no significant tendency for the pressure to decrease over time, indicating that 15 seconds is sufficient time for the pressure to equilibrate. If the timescale of equilibration were, in fact, significantly longer than a few minutes, the precision of this technique would clearly be limited by the stability of the measurement system (including the room temperature).

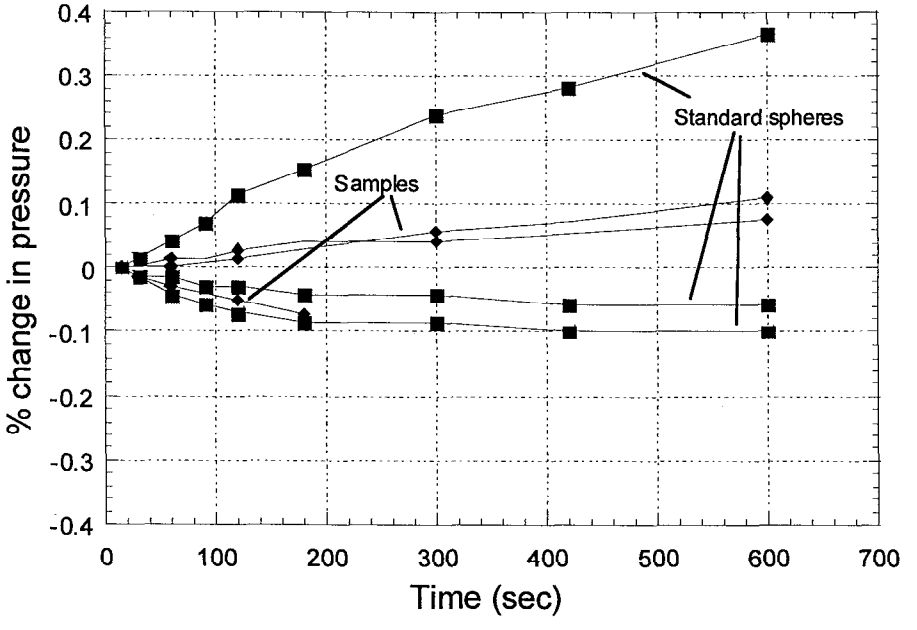

Figure 2. Percentage changes in pressure of the Multipycnometer® as a function of time relative to the pressure at 15 seconds. The drift is primarily attributed to small changes in the temperature of the room and apparatus during the measurements.

Porosity calculations

The total porosity of the samples was calculated by dividing the bulk density by the theoretical density and subtracting the result from one. Similarly, the closed porosity was calculated by dividing the "pycnometer density" by the theoretical density and subtracting the result from one. The open porosity is then simply the difference between the total porosity and the closed porosity. All three values (expressed as a percentage) are tabulated for each sample in Table 3.

Table 3. Density and porosity data for ceramic samples. Errors are 1 standard deviation.

Sample ID	Nominal sintering temp. (deg. C)	Mass (g)	Theoretical density (g/cc)	Geometric volume (cc)	+/- (cc)	Bulk density g/cc	Total porosity	+/-	Pycnometer volume (cc)	+/- (cc)	Pycnometer density (g/cc)	Closed porosity	error	Open porosity	error	Closed/total porosity	error
178#1	1350	2.6259	5.4	0.777	0.008	3.380	37.40%	0.65%	0.490	0.002	5.359	0.77%	0.34%	36.63%	0.99%	0.020	0.009
178#2	1350	3.3990	5.4	0.834	0.058	4.078	24.49%	5.25%	0.662	0.002	5.134	4.93%	0.32%	19.56%	5.56%	0.201	0.045
178#3	1350	2.1581	5.4	0.466	0.008	4.631	14.24%	1.53%	0.438	0.003	4.929	8.72%	0.67%	5.52%	2.20%	0.612	0.081
178#4	1350	2.7751	5.4	0.568	0.003	4.882	9.58%	0.47%	0.550	0.002	5.048	6.52%	0.35%	3.06%	0.82%	0.680	0.050
178#5	1350	3.4109	5.4	0.697	0.004	4.892	9.41%	0.57%	0.688	0.001	4.961	8.13%	0.11%	1.28%	0.68%	0.864	0.054
178#6	1350	2.8869	5.4	0.596	0.004	4.842	10.33%	0.57%	0.581	0.005	4.972	7.93%	0.82%	2.40%	1.39%	0.768	0.090
178#7	1350	2.5827	5.4	0.532	0.003	4.858	10.04%	0.53%	0.519	0.001	4.973	7.91%	0.16%	2.14%	0.68%	0.787	0.044
178#8	1350	2.4974	5.4	0.512	0.003	4.877	9.68%	0.58%	0.505	0.003	4.944	8.44%	0.50%	1.24%	1.08%	0.872	0.074
178#9	1350	1.6662	5.4	0.345	0.003	4.828	10.59%	0.76%	0.340	0.004	4.904	9.19%	0.96%	1.39%	1.72%	0.869	0.110
178#10	1350	1.6445	5.4	0.416	0.018	3.957	26.73%	3.24%	0.329	0.006	5.005	7.31%	1.57%	19.42%	4.81%	0.273	0.067
178#11	1350	3.4483	5.4	1.056	0.062	3.265	39.54%	3.56%	0.664	0.004	5.194	3.81%	0.58%	35.73%	4.14%	0.096	0.017
178#12	1350	2.2544	5.4	0.798	0.039	2.824	47.69%	2.55%	0.432	0.008	5.217	3.38%	1.82%	44.31%	4.37%	0.071	0.038
183#1	1400	2.7295	5.4	0.571	0.003	4.783	11.43%	0.41%	0.545	0.007	5.008	7.25%	1.15%	4.18%	1.56%	0.635	0.103
183#2	1400	2.3416	5.4	0.490	0.002	4.778	11.52%	0.38%	0.470	0.006	4.980	7.78%	1.08%	3.75%	1.47%	0.675	0.097
183#3	1400	1.8282	5.4	0.384	0.003	4.761	11.84%	0.60%	0.364	0.006	5.023	6.98%	1.47%	4.85%	2.06%	0.590	0.127
183#4	1400	2.2741	5.4	0.475	0.002	4.787	11.36%	0.34%	0.458	0.004	4.964	8.08%	0.78%	3.28%	1.12%	0.711	0.072
183#5	1400	2.0425	5.4	0.428	0.004	4.774	11.60%	0.76%	0.409	0.005	4.992	7.56%	1.11%	4.04%	1.86%	0.652	0.104
183#6	1400	1.9332	5.4	0.411	0.006	4.704	12.89%	1.26%	0.388	0.003	4.985	7.68%	0.78%	5.21%	2.04%	0.596	0.084
183#7	1400	2.5863	5.4	0.538	0.003	4.804	11.05%	0.50%	0.520	0.001	4.971	7.95%	0.19%	3.09%	0.68%	0.720	0.036
183#8	1400	2.1889	5.4	0.456	0.002	4.803	11.06%	0.44%	0.436	0.005	5.024	6.96%	1.06%	4.10%	1.51%	0.629	0.099
183#9	1400	2.1146	5.4	0.439	0.002	4.821	10.71%	0.33%	0.421	0.004	5.020	7.03%	0.83%	3.68%	1.16%	0.656	0.080
183#10	1400	2.2761	5.4	0.476	0.006	4.785	11.38%	1.16%	0.452	0.005	5.039	6.68%	1.00%	4.70%	2.15%	0.587	0.106
183#11	1400	2.3009	5.4	0.517	0.003	4.454	17.51%	0.51%	0.456	0.004	5.045	6.58%	0.77%	10.93%	1.28%	0.376	0.045
183#12	1400	2.7317	5.4	0.568	0.006	4.812	10.89%	0.90%	0.545	0.003	5.010	7.22%	0.52%	3.68%	1.42%	0.662	0.072
BR2-40	1350	4.6972	4.92	0.982	0.051	4.781	2.82%	5.01%	0.977	0.003	4.810	2.24%	0.35%	0.58%	5.36%	0.793	1.414

Results and Discussion

The total porosities of the samples range from 47.7% to 2.8%, the close porosities ranged from 8.7% to 0.8%, and the open porosities range from 44.3% to 0.6%. Figures 3 through 5 show that these variations are correlated in the expected manner.

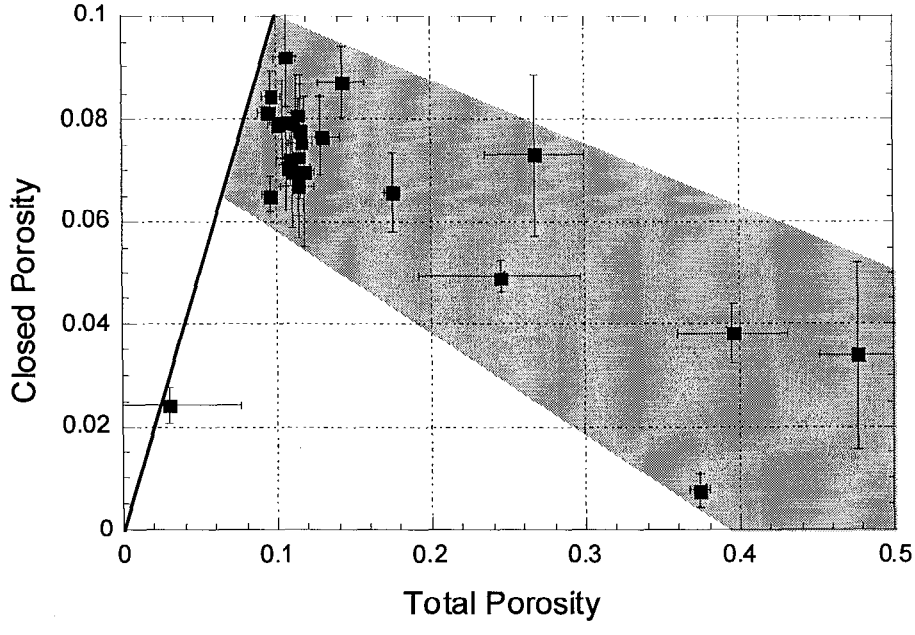

Figure 3. Plot of closed porosity *vs.* total porosity for the ceramic samples. The critical porosity at which interconnected porosity starts to develop is around 8% total porosity.

Figure 3 is a plot of the closed porosity *vs.* the total porosity. A comparison of this figure with Figure 1 shows that the data are consistent with the expected pattern: at porosities less than some critical value, the closed porosity is approximately equal to the total porosity, while above the critical value, the closed porosity decreases with increasing total porosity. In the case of the ceramic, the critical porosity appears to lie somewhere between 5 and 10% total porosity.

Figure 4 is another way of portraying the same data. In this case, the figure shows the fraction of the total porosity that is closed as a function of the total porosity. As with the other methods of portraying the data, a critical value of the porosity of ~8% is indicated. The curve is a power-law fit to the data, excluding the data point at 2.8% total porosity. The errors on this data point are quite large because of the large relative error on the determination of the bulk density of this sample. No particular significance should be assigned to the fit; it is included on the figure as a guide to the general trend of the data.

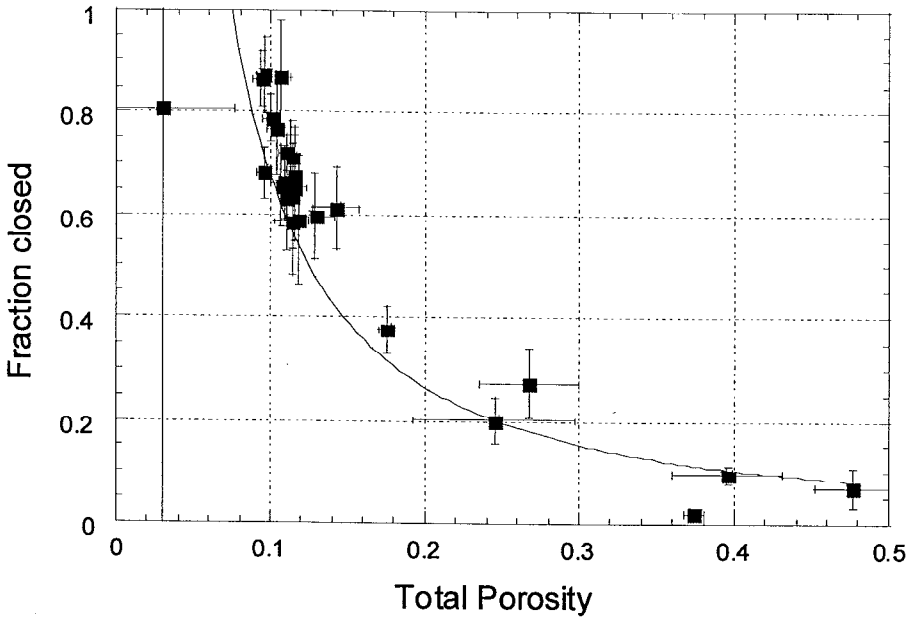

Figure 4. Fraction of porosity that is closed plotted against total porosity. Curve is a power-law fit to the data points with total porosity >8%.

Figure 5 is a plot of the open porosity *vs.* the total porosity. As expected nearly all of the porosity is open at high total porosity, and open porosity makes up a decreasing fraction of the total as the total porosity decreases. Again, the data are consistent with a critical porosity of approximately 8%; below ~8% total porosity, nearly all the porosity is closed.

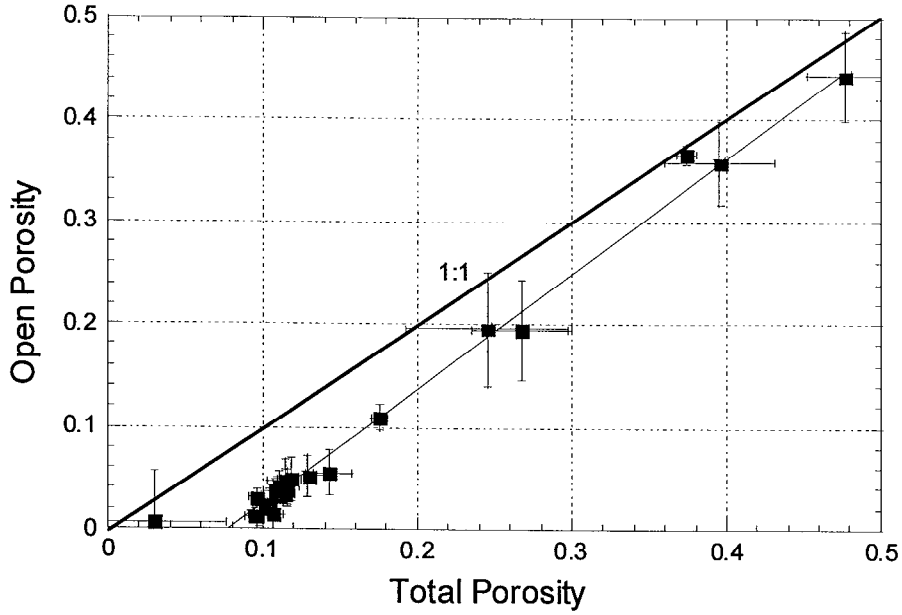

Figure 5a. Plot of open porosity *vs.* total porosity for the ceramic samples

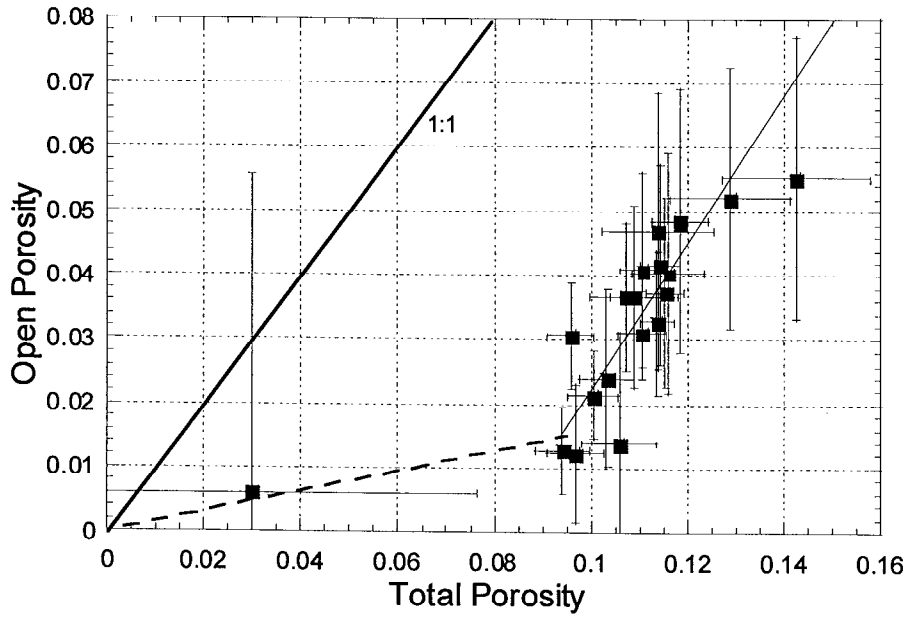

Figure 5b. Expanded view of low porosity region of Figure 5a

Relationship Between Open Porosity and Surface Area

The surfaces of the pores in an interconnected network that intersects the surface of the wasteform represent additional surface area that can react with groundwater under repository conditions. It is therefore of interest to evaluate how this "accessible" surface area varies as the open porosity varies. A crude estimate of this relationship can be obtained by assuming that the interconnected porosity can be represented by a series of "tubes" with radius r and total length l. For simplicity, initially we will assume that the wasteform fragments are spheres with radius R. Then, the open porosity, ϕ_o, can be expressed as:

$$\begin{aligned} \phi_o &= \text{(volume of open pores)/(total sample volume)} \\ &= 3r^2 l /4R^3, \end{aligned}$$

from which we obtain the total length of the open porosity structure:

$$l = 4\phi_o R^3/3r^2$$

The geometric (external) surface area, A_G of the spherical fragment is:

$$A_G = 4\pi R^2,$$

and the "internal" surface area due to the interconnected porosity is:

$$\begin{aligned} A_I &= 2\pi r l \\ &= 8\pi\phi_o R^3/3r. \end{aligned}$$

The factor, Δ_{sphere}, by which the accessible surface area is increased by the existence of the open porosity, is given by:

$$(A_G + A_I)/ A_G \equiv \Delta_{sphere} = 1 + 2\phi_o R/3r.$$

This analysis is not limited to a spherical geometry for the fragment. The same analysis using a cylindrical geometry yields $\Delta_{cyl} = (1 + \phi_o RA/r(1+A))$, where R is the radius of the cylinder and A is the aspect ratio of the cylinder (the ratio of the height to the radius). Similarly, assuming the wasteform has a cubical geometry yields $\Delta_{cube} = (1 + \pi\phi_o H/3r)$, where H is the length of the side of the cubes. In all cases, the increase in surface area is proportional to the open porosity multiplied by the ratio of the characteristic size of the wasteform fragments to the characteristic aperture size of the pores, *i.e.*, the factor $\phi_o R/r$. For a given pore and fragment size ratio, doubling the open porosity will nearly double the accessible internal surface area.

These scaling relationships are shown in Figure 6, in which contours of the quantity $(1 + \phi_o R/r)$ are plotted as a function of total porosity and log(R/r). For the purposes of making

this diagram, the open porosity was assumed to depend on the total porosity in the following manner:

$$\phi_{total} < 9\%: \ \phi_o = \phi_{total}/6 \text{ and } \quad \phi_{total} \geq 9\%: \ \phi_o = 1.15\phi_{total} - 0.093$$

These relationships are consistent with the data shown in Figure 5b.

The Pu ceramic will most likely have a total porosity of less than about 13%, and a grain size between 5 and 15 microns. Assuming that the pore size is approximately that of the grain size, and fragments that range in size between 1 and 5 cm. results in a range of R/r values between 1000 and 10000 (log(R/r) between 3 and 4). This region of parameter space is highlighted in Figure 6. The most likely value of R/r will be around 2000 (2cm/10microns, log(R/r) ~ 3.3).

The model relationships between open porosity and surface area described above predict that the ratio of accessible surface area to the geometric surface area of a fragment could be as high as a few thousand. It is important to note, however, that all monolithic (*i.e.*, uncrushed) samples that have been tested to date have porosities and fragment sizes that are more or less typical of what is expected for in-repository conditions. Therefore, the test results on monolithic specimens already reflect the increase in surface area due to open porosity.

It is also important to note that under nearly all conditions, the leach rate of elements from a waste package (*i.e.*, the removal rate, not the degradation rate of the ceramic) will be independent of the wasteform surface area. This is because the elements composing the ceramic have low to extremely low solubilities, and their transport will be "solubility limited", not "dissolution rate limited". For solubility limited releases, it is incorrect to use the surface area as a scaling factor in calculating elemental release rates. Furthermore, the actual dissolution rates of the minerals in the ceramic should be depend on solution chemistry, with the dissolution rate decreasing as the concentration of the dissolved components builds up in solution. Diffusion (as opposed to advection) will essentially be the only mechanism for transport of dissolved components through a fluid phase occupying the connected porosity of the ceramic. This "internal" solution phase should contain higher concentrations of dissolved components than will the free solution external to the wasteform (which is potentially subject to a "flushing" process as groundwater enters and leaves a failed package), and the dissolution rate of the internal surfaces will be correspondingly slower than that of the exterior surfaces. In the extreme limit, the internal fluid phase could approach equilibrium with the ceramic minerals, and the dissolution rate of the internal surfaces would approach zero.

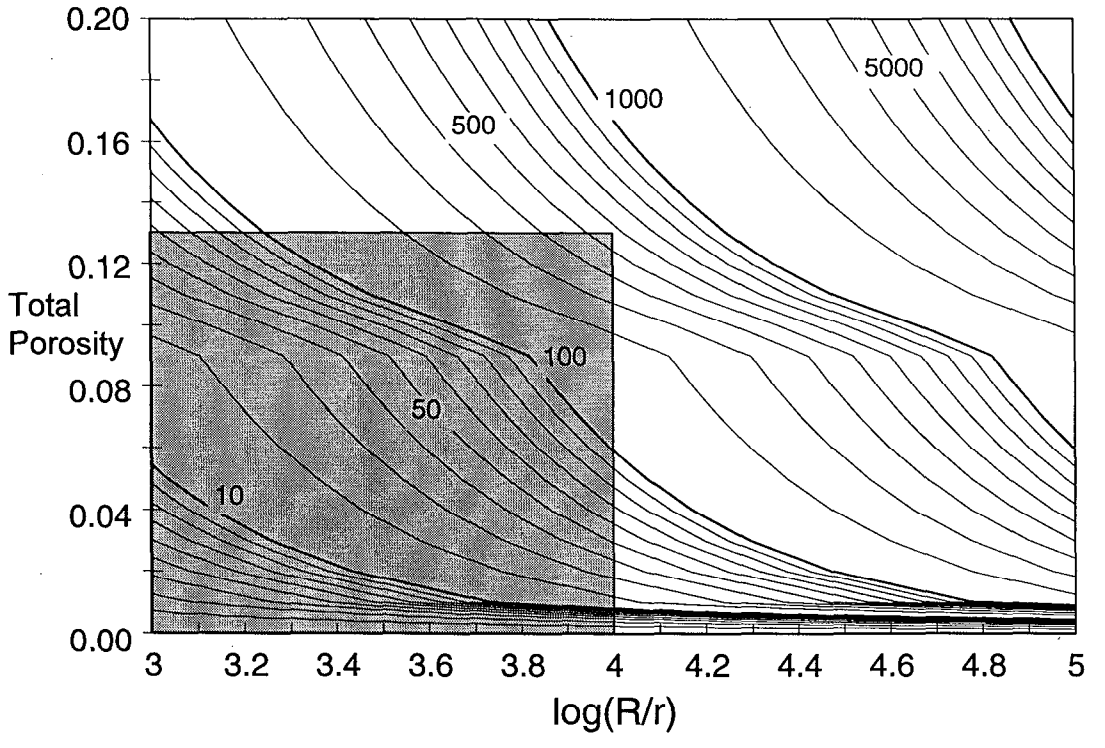

Figure 6. Contour plot of $(1+R\phi_c/r)$, the scaling factor by which open porosity increases the surface area. Shaded area is the region of parameter space likely to be occupied by the Pu ceramic form.

Suggested Improvements for Future Work

In conducting this work, several items were noted that would improve the results, or provide more definitive data on the actual Pu-bearing ceramic. These observations are listed below.

1. Characterization work on similar fully nonradioactive, analog ceramic (Ce substituting for both Pu and U), ceramics has shown that perovskite is almost always present in the final ceramic, probably because of the reduction of Ce^{4+} to Ce^{3+}. This phase is not present in the U- and Pu-bearing version of the ceramic. Ultimately, similar measurements will need to be made on actual samples of the Pu-bearing ceramic to confirm the porosity relationships.

2. The use of the natural temperature gradient of the furnace to achieve variable densities/extent of reaction is convenient, but is not a well controlled procedure. Individual pellets may even have a porosity gradient across them corresponding to the temperature gradient to which they were exposed during sintering. Future work should be performed on ceramic samples that have been sintered in a series of runs at different, known temperatures in the "hot spot" of a calibrated oven.

3. Because the low-density pellets were exposed to lower sintering temperatures, it is likely that they are not fully reacted (*i.e.*, that the mineralogy of these pellets does not correspond to the equilibrium phase assemblage, and that there is unreacted or partially reacted starting material present). This difference will likely affect both grain size and the morphology of the grains, and may thus affect the porosity relationships. A series of samples should be prepared by re-sintering pellets formed from a starting material prepared by grinding/milling fully reacted ceramic. Sintering these pellets at different temperatures should result in pellets with different porosities, and possibly different grain sizes, but with identical mineralogy. Measurements of the total and open porosity should be performed on these samples to eliminate the effects of variable mineralogy. A parallel set of samples for measurement should be prepared from the normal oxide and hydroxide starting materials so that the effects of incomplete reaction on the porosity relationships can be assessed.

4. The presence of silica in some of the Pu feedstreams will give rise to a liquid silicate phase in the ceramic during sintering. This fluid phase has the potential to modify the porosity network. Porosity relationships should be determined on a series of samples containing silica impurities to explore the effects of a melt phase.

5. The major source of error in the calculations in this work is the determination of the geometric volume of the samples. The as-fabricated pellets are not perfect right circular cylinders, which makes it difficult to make an accurate determination of the volume using simple direct dimensional measurements. A better method for determining the geometric volume is desireable. Improvements might involve machining/cutting/grinding the as-fabricated pellets to a uniform geometry, or might entail a completely different method for volume determination (*e.g.* an Archimedes principal-based method).

Conclusions

This work was intended as a scoping study to establish the basic relationships between open and closed porosity in the ceramic under consideration for Pu immobilization. Of primary interest is the critical porosity at which the pore network "closes off" and consists of a series of isolated pores. This was found to occur at a total porosity of approximately 8%, a value consistent with the behavior of many other materials. It is expected that the critical porosity will be relatively insensitive to the range of grain size, compositional, and mineralogical variations that are likely to be present in the Pu ceramic, and this value should provide a reasonable working estimate for planning purposes.

References

Isichenko, M. B., 1992, Percolation, statistical topography, and transport in random media. *Rev. Mod. Phys.*, v64, #4, pp961-1043.